https://doi.org/10.2352/ISSN.2470-1173.2017.8.MAAP-274

A Normal Vector and BTF Profile Measurement System Using a Correlation Camera and Scanning Dome Illumination

Akira Kimachi, Motonori Doi, Shogo Nishi; Faculty of Information and Communication Engineering, Osaka Electro-Communication University; Neyagawa, Japan

Abstract

A system for simultaneously measuring surface normal vectors and BTF (bidirectional texture function) profiles of an object is proposed. This system consists of a correlation camera and a spherical scanning light source. The system can compress BTF measurement in one dimension of incidence direction to a single image frame, as well as measure a profile of the BTF under the scanning light source just from a single image frame. Experimental results on an implemented system demonstrate the feasibility of the proposed system.

Introduction

Realistic image rendering has recently drawn great attention in such applications as digital heritage, training simulators, motion pictures, video games and so on. It requires information on the object in regard to not only three-dimensional (3-D) shape, position, and pose, but also light reflection on the surface. In order to reproduce an image of a real object, it is necessary to accurately measure 3-D information and the property of light reflection of the object at the same time. Measurement of light reflection properties does not seem to have been studied as actively as 3-D measurement in computer vision, and regarding simultaneous measurement of both, less achievement can be found. Reflection of light on the surface of an object is represented as a bidirectional reflectance distribution function (BRDF) defined at a point, or as a bidirectional texture function (BTF) defined over a 2-D area. To measure a BRDF or BTF, we suffer from a trade-off between resolution and time because of the high dimensionality of them.

This trade-off can be alleviated by use of a video camera, whose capability of 2-D parallel sensing can compress two of the four or six parameter dimensions to a single image frame. For BRDF measurement, some methods employ a sphere with uniform reflectance as the object to sample the incidence and viewing directions by the image sensor [1]. It requires mechanically rotating the light source and the camera to change the incidence and viewing directions over a wide range. Other methods employ a digital projector and an ellipsoidal mirror, and sample the incidence and viewing directions by pixels of the projector and the camera [2], achieving short measurement time without no mechanical parts. There is also a method that did not use a camera but a dome of LEDs instead [3]. The LEDs not only work as light sources but also are used as photodetectors, thus sampling the incidence and viewing directions by the arrangement of themselves on the internal dome surface. In these methods, we need an extra 2-D scan of the object in order to obtain a BTF, and an additional apparatus for 3-D measurement. BTFs are usually measured simply by rotating or moving the object, camera and light source to change relative geometry among them [4]. This is a straightforward approach directly affected by the trade-off. Simultaneous measurement of the 3-D shape and BTF were reported in references [5, 6]. They measure the 3-D shape by pattern projection with a digital projector, and acquire images for different incidence and viewing directions by rotating the object or manually moving the light source and the camera. Although they obtained BTFs for all incidence and viewing directions, the sampling of the directions was not dense, and the model of specular reflection was assumed uniform all over the object.

In this paper, we propose a system for simultaneously measuring surface normal vectors and BTF profiles of an object with high angular resolution and shorter measurement time than previous methods. The key components of this system are the correlation camera [7] and a scanning spherical light source, though in the prototype system the light source was realized as a dome or a hemisphere. The correlation camera captures the images of temporal correlations between the intensity signal of the light reflected on the object and complex sinusoidal reference signals, while the scanning light source rotates about the camera axis once in a frame time. This sensing architecture enables the system to compress BTF measurement in one dimension of incidence direction to a single image frame. In addition, the parameters of specular reflection for some latitude of the scanning light source are estimated just from a single frame set of output images, producing a 1-D "BTF profile" of a 6-D BTF manifold over a certain range of incidence direction for that latitude of the light source.

The remainder of the paper describes the principle and implementation of the proposed system, shows the results obtained on the experimental system, and finally concludes the paper.

Measurement system

Structure

Figure 1 illustrates a schematic of the system for measuring surface normal vectors and BTF profiles of an object. The system consists of a correlation camera [7] and a scanning light source.

The correlation camera produces the temporal correlation between the intensity signal of incoming light $f(x,y,t)$ and three global reference signals at each pixel (x,y) in every frame time T. This system employs three-phase sinusoidal reference signals $\cos[k\omega_0 t + \frac{2\pi}{3}(l-1)]$ $(l = 1,2,3)$, where $\omega_0 = 2\pi/T$ denotes the angular frame frequency and k (≥ 1) is an integer. Under these reference signals, the output images $Q_l(x,y)$ $(l = 1,2,3)$ of the correlation camera are given by

$$\begin{bmatrix} Q_1(x,y) \\ Q_2(x,y) \\ Q_3(x,y) \end{bmatrix} = \rho \int_{-T/2}^{T/2} f(x,y,t) \begin{bmatrix} \cos k\omega_0 t \\ \cos(k\omega_0 t + \frac{2\pi}{3}) \\ \cos(k\omega_0 t + \frac{4\pi}{3}) \end{bmatrix} dt$$

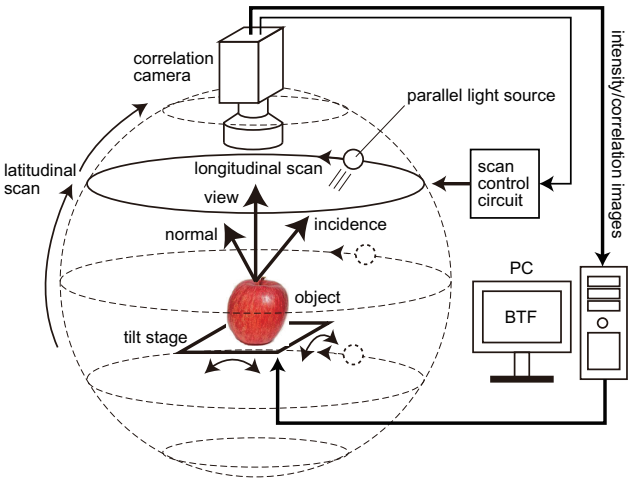

Figure 1. *A schematic of the proposed measurement system.*

$$+\frac{1}{3}\int_{-T/2}^{T/2} f(x,y,t)dt \begin{bmatrix}1\\1\\1\end{bmatrix} \tag{1}$$

where ρ denotes the relative gain of the first component. Defining

$$g_0(x,y) \triangleq \int_{-T/2}^{T/2} f(x,y,t)dt$$

$$g_k(x,y) \triangleq \int_{-T/2}^{T/2} f(x,y,t)e^{-jk\omega_0 t}dt$$

we can convert $Q_k(x,y)$ to the temporal correlation $g_k(x,y)$ with a complex sinusoidal reference signal $e^{-jk\omega_0 t}$ and the average intensity $g_0(x,y)$ as

$$\begin{bmatrix}\Re\{g_k(x,y)\}\\ \Im\{g_k(x,y)\}\\ g_0(x,y)\end{bmatrix} = \begin{bmatrix}\frac{2}{3\rho} & -\frac{1}{3\rho} & -\frac{1}{3\rho}\\ 0 & \frac{1}{\sqrt{3}\rho} & -\frac{1}{\sqrt{3}\rho}\\ 1 & 1 & 1\end{bmatrix}\begin{bmatrix}Q_1(x,y)\\ Q_2(x,y)\\ Q_3(x,y)\end{bmatrix} \tag{2}$$

The scanning light source consists of a spherical shell and a light source that moves along the internal surface of the shell while projecting the light toward its center. The system geometry is defined in reference to this shell, which is regarded as a globe. The object is placed at the origin and imaged by the correlation camera from the north pole through a hole on the shell. The light flux on the object can be made nearly parallel by making the radius of the shell much larger than the field of view. The light source rotates once along the line of some latitude of the shell at an angular velocity ω_0 during a single image frame of the correlation camera, and shifts from the lower to the higher latitude frame by frame. After the light source has scanned the whole shell and a sequence of images has been acquired, the pose of the object is changed and the same process of light-source scanning and image acquisition is repeated.

From the sequence of output images, the normal vector and the BTF profiles for the surface of the object are measured pixel by pixel, without any interpixel computation. In this regard, the pixel coordinate (x,y) is omitted in the principle below.

Correlation imaging under light-source scanning

Let θ_m and (θ_n,ϕ_n) respectively denote the m-th latitude of the scanning light source, and the latitude and longitude of the surface normal vector at a point on the object, as illustrated in Figure 2. θ_m varies from the south to the north pole as $-\frac{1}{2}\pi < \theta_m < \frac{1}{2}\pi$, whereas θ_n is limited to $0 \le \theta_n < \frac{1}{2}\pi$ because the surface of the object must face the correlation camera for valid measurement. The position of the light source relative to the object's surface is classified into three cases, as depicted in Figure 3:

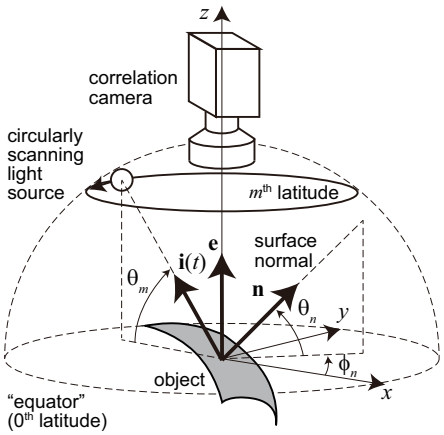

Figure 2. *Imaging geometry of the measurement system.*

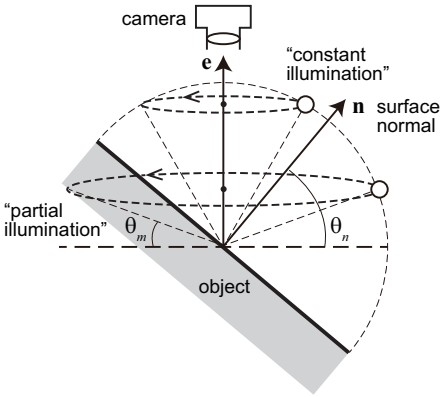

Figure 3. *Position of the scanning light source relative to the object's surface.*

1. "constant illumination" ($\theta_m \ge \frac{1}{2}\pi - \theta_n$), where the light source always illuminates the surface from the front side;
2. "partial illumination" ($\theta_n - \frac{1}{2}\pi < \theta_m < \frac{1}{2}\pi - \theta_n$), where the light source hides behind the surface in some portion of the frame time; and
3. "no illumination" ($\theta_m \le \theta_n - \frac{1}{2}\pi$), where the light source is always behind the surface throughout the frame time.

The "no illumination" case is not considered because it does not enable imaging.

Let $f_m(t)$ denote the intensity signal of the light that is reflected on the object and enters the correlation camera. $f_m(t)$ is decomposed into a diffuse reflection component $d_m(t)$ and a specular reflection component $s_m(t)$ as

$$f_m(t) = d_m(t) + s_m(t) \tag{3}$$

From the cosine law for Lambertian diffuse reflection, $d_m(t)$ is expressed as

$$d_m(t) = w(t,\theta_m,\theta_n,\phi_n)$$

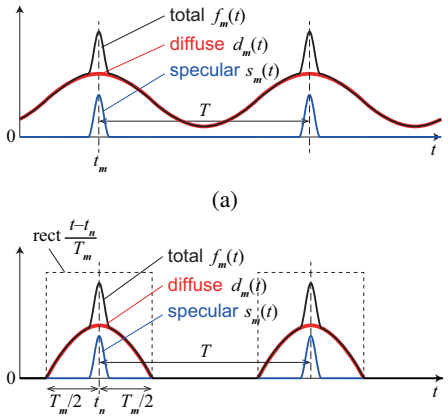

Figure 4. *Models of the intensity signal of reflected light. (a) "Constant illumination" case. (b) "Partial illumination" case.*

$$\cdot \quad E_0 R[\cos\theta_m \cos\theta_n \cos(\omega_0 t - \phi_n) + \sin\theta_m \sin\theta_n] \tag{4}$$

where E_0 and R denote the intensity of the light source and the diffuse reflectance of the object, respectively, and $w(t,\theta_m,\theta_n,\phi_n)$ denotes a window function of a period T that accounts for the three cases of relative position of the light source as

$$w(t,\theta_m,\theta_n,\phi_n) \triangleq \begin{cases} 1, & \theta_m \geq \frac{1}{2}\pi - \theta_n \\ \mathrm{rect}\left(\dfrac{(t-t_n+\frac{1}{2}T) \bmod T - \frac{1}{2}T}{T_m}\right), & \theta_m < \left|\frac{1}{2}\pi - \theta_n\right| \\ 0, & \theta_m \leq \theta_n - \frac{1}{2}\pi \end{cases} \tag{5}$$

In Eq. (5), $\mathrm{rect}(u)$ denotes a unit rectangular window function

$$\mathrm{rect}(u) \triangleq \begin{cases} 1, & -\frac{1}{2} \leq u \leq \frac{1}{2} \\ 0, & \text{otherwise} \end{cases}$$

T_m denotes the duration in which the light source illuminates the surface from the front side, defined by

$$T_m \triangleq \frac{2}{\omega_0}\cos^{-1}(-\tan\theta_m \tan\theta_n) \tag{6}$$

$t_n \triangleq \phi_n/\omega_0$ denotes the center of the window function, which turns out to coincide with the peak time of the sinusoidal function in Eq. (4).

For the specular reflection component $s_m(t)$, which has periodic peaks in every T, we assume a wrapped Gaussian distribution defined by

$$s_m(t) = A_m \sum_{l=-\infty}^{\infty} \frac{1}{\sqrt{2\pi}\sigma_m} \exp\left[-\frac{(t-t_m-lT)^2}{2\sigma_m^2}\right] \tag{7}$$

In Eq. (7), A_m, σ_m and t_m respectively denote the height, width and time of the specular peak, and the subscript m is added because the waveform of the specular reflection component varies for different latitude θ_m. In a strict sense, the same window function $w(t,\theta_m,\theta_n,\phi_n)$ is multiplied to the wrapped Gaussian distribution in Eq. (7), but can be neglected for a sufficiently narrow peak width $\sigma_m \ll T_m$, which is usually the case in practice. Figure 4 depicts typical waveforms of $f_m(t)$, $d_m(t)$ and $s_m(t)$ for the "constant illumination" and "partial illumination" cases.

For the incoming light $f_m(t)$ in Eq. (3), each pixel of the correlation camera outputs the average intensity g_{m0} and the temporal correlation g_{mk} with a complex sinusoidal reference signal $e^{-jk\omega_0 t}$ $(k = 1,2,\ldots)$ in every frame as

$$g_{m0} \triangleq \int_{-T/2}^{T/2} f_m(t)dt \tag{8}$$

$$g_{mk} \triangleq \int_{-T/2}^{T/2} f_m(t)e^{-jk\omega_0 t}dt \tag{9}$$

Substituting Eqs. (3), (4) and (7) into Eqs. (8) and (9) yields

$$g_{mk} = D_{mk} + S_{mk} \tag{10}$$

where

$$D_{mk} \triangleq \int_{-T/2}^{T/2} d_m(t)e^{-jk\omega_0 t}dt = \begin{cases} C_{mk}, & \theta_m \geq \frac{1}{2}\pi - \theta_n \\ \sum_{l=-1}^{1} W_{m,k-l}C_{ml}, & \theta_m < \left|\frac{1}{2}\pi - \theta_n\right| \end{cases} \tag{11}$$

$$C_{mk} \triangleq \frac{1}{2}TE_0R\cos\theta_m\cos\theta_n(e^{-j\phi_n}\delta_{k1} + e^{j\phi_n}\delta_{k,-1}) + TE_0R\sin\theta_m\sin\theta_n\delta_{k0} \tag{12}$$

$$W_{mk} \triangleq \frac{1}{T}\int_{-T/2}^{-T/2} w(t,\theta_m,\theta_n,\phi_n)e^{-jk\omega_0 t}dt = \frac{T_m}{T}e^{-jk\omega_0 t_n}\mathrm{sinc}\left(\frac{1}{2}k\omega_0 T_m\right) \tag{13}$$

$$S_{mk} \triangleq \int_{-T/2}^{T/2} s_m(t)e^{-jk\omega_0 t}dt = A_m e^{-jk\omega_0 t_m}e^{-\frac{1}{2}(k\sigma_m\omega_0)^2} \tag{14}$$

and δ_{kl} and $\mathrm{sinc}(u) \triangleq \sin u/u$ respectively denote the Kronecker's delta and a sinc function. D_{mk} and S_{mk} are equivalent to the k-th order Fourier coefficients of the diffuse and specular reflection components $d_m(t)$ and $s_m(t)$, respectively. Note that

$$C_{mk} = \begin{cases} TE_0R\sin\theta_m\sin\theta_n, & k=0 \\ \frac{1}{2}TE_0Re^{-j\phi_n}\cos\theta_m\cos\theta_n, & k=1 \\ 0, & k\geq 2 \end{cases} \tag{15}$$

Parameter estimation algorithm

The goal of the proposed system is to estimate, from the set of g_{m0} and g_{mk} obtained for different latitude θ_m of the scanning light source, the surface normal direction (θ_n,ϕ_n) and the diffuse reflectance R, which are invariant to θ_m, and the parameters of the specular compoent A_m, σ_m and t_m, which vary with θ_m. From Eqs. (11)–(15) we can argue that:

1. The parameters R and (θ_n,ϕ_n) can be estimated from g_{m0} and g_{m1} if g_{m0} is sufficiently large and $g_{m2} \simeq 0$.
2. This condition occurs when the specular reflection component S_{mk} is almost missing and the lighting condition is "constant illumination" $(\theta_m \geq \frac{1}{2}\pi - \theta_n)$.
3. This condition is highly likely to occur for some θ_m because the camera can capture specular reflection only for a limited range of incident direction.
4. The specular reflection component S_{mk} can be separated from g_{mk} by estimating the diffuse reflection component D_{mk} from R and (θ_n,ϕ_n) and then subtracting them.

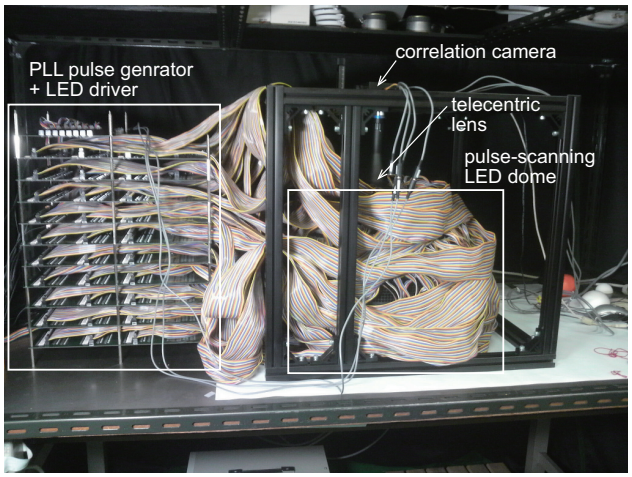

Figure 5. *A photograph of the fabricated scanning light source.*

The above idea of separating the diffuse and specular components depending on the values of g_{m0}, g_{m1} and g_{m2} have similarities to that proposed for a real-time imaging system for surface normal vectors using the correlation camera [8, 9]. Based on this argument, we devise an algorithm for esitmating these parameters from at least g_{m0}, g_{m1} and g_{m2} as follows:

1. Set $m = 0$.
2. If $g_{m0} < g_{0\min}$, then put the label "no illumination" and go to Step 4.
3. If $|g_{m2}| < g_{2\min}$, then assume $S_{mk} \simeq 0$ $(k = 0,1,2)$, $g_{m0} \simeq D_{m0} \simeq C_{m0}$ and $g_{m1} \simeq D_{m1} \simeq C_{m1}$, and compute the estimates of diffuse reflectance $\hat{R}$ and surface normal direction $(\hat{\theta}_n, \hat{\phi}_n)$ as
$$\hat{R}_m = \frac{1}{TE_0}\sqrt{\frac{g_{m0}^2}{\sin^2\theta_m} + \frac{4|g_{m1}|^2}{\cos^2\theta_m}}$$
$$\hat{\theta}_{nm} = \tan^{-1}\frac{g_{m0}}{2|g_{m1}|\tan\theta_m}, \quad \hat{\phi}_{nm} = -\angle g_{m1}$$
4. Increment m and repeat Steps 2–4 for all m.
5. Compute the averages $\hat{R}$, $\hat{\theta}_n$ and $\hat{\phi}_n$ of the estimated parameters $\hat{R}_m$, $\hat{\theta}_{nm}$ and $\hat{\phi}_{nm}$, respectively.
6. Set $m = 0$.
7. If the label is "no illumination", then go to Step 11.
8. Compute the estimates of the diffuse reflection component $\hat{D}_{m0}$, $\hat{D}_{m1}$ and $\hat{D}_{m2}$ from $\hat{R}$, $\hat{\theta}_n$ and $\hat{\phi}_n$ by Eqs. (6) and (11)–(13).
9. Estimate the specular reflection component as $\hat{S}_{mk} = g_{mk} - \hat{D}_{mk}$ $(k = 0,1,2)$.
10. Compute the estimates of specular reflection parametes $\hat{A}_m$, $\hat{\sigma}_m$ and $\hat{t}_m$ from $\hat{S}_{m0}$, $\hat{S}_{m1}$ and $\hat{S}_{m2}$ by applying a least-squares method to $\log|S_{mk}|$ and $\angle S_{mk}$ as
$$\hat{t}_m = -\frac{1}{\omega_0 \sum_{k=1}^{2} 1}\sum_{k=1}^{2}\frac{\angle g_{mk}}{k}, \quad \hat{A}_m = e^a, \quad \hat{\sigma}_m = \frac{\sqrt{2b}}{\omega_0}$$
$$\begin{bmatrix} a \\ b \end{bmatrix} = \begin{bmatrix} \sum_{k=0}^{2} 1 & -\sum_{k=0}^{2} k^2 \\ -\sum_{k=0}^{2} k^2 & \sum_{k=0}^{2} k^4 \end{bmatrix}^{-1} \begin{bmatrix} \sum_{k=0}^{2} \log|\hat{S}_{mk}| \\ \sum_{k=0}^{2} k^2 \log|\hat{S}_{mk}| \end{bmatrix}$$
11. Increment m and repeat Steps 8–10 for all m.

The above algorithm estimates the specular reflection parameters A_m, σ_m and t_m for a variety of incident directions of the light source along a latitude line at θ_m, virtually from just a single frame set of correlation images g_{mk} $(k = 0,1,2)$, as well as simultaneously measures the diffuse reflectance R and the surface normal direction (θ_n, ϕ_n) pixel by pixel. These parameters form a 1-D profile with respect to θ_m out of a 6-D BTF manifold.

Specifications of the LED dome scanning light source.

Dome radius	200 mm									
LED	white, 35000 mcd, 64 mW									
Latitude θ_m	15°	20°	25°	30°	35°	40°	45°	50°	55°	60°
No. of LEDs	209	203	196	187	177	165	153	139	124	108

Specifications of the correlation camera.

No. of pixels	704×512
Pixel dimension	$12\ \mu\text{m} \times 12\ \mu\text{m}$
Frame rate	14.1 fps
Exposure	Rolling shutter
Lens	Telecentric $0.16\times$
Field of view	~ 50 mm diameter
Imaging distance	~ 170 mm

Fabrication and implementation

Figure 5 shows the scanning light source fabricated in our laboratory. Instead of a single rotating light source, white light emitting diodes (LEDs) are used and embedded in an aluminum spheric shell densely along each latitude line. As a first step, the shell is fabricated as a dome, i.e. it has the northern hemisphere only, and the southern hemisphere will be fabricated later. The LEDs on each latitude line are sequentially turned on to realize a scanning light source, controlled by a phase-locked loop (PLL) and a parallel shift register in synchrony to the frame signal of the correlation camera. Table 1 lists specifications of the scanning light source.

The correlation camera, hung above the LED dome, has specifications as listed in Table 2. It can simultaneously output either g_{m0} and g_{m1} or g_{m0} and g_{m2} in a checkered manner from every other pixel, though the resolution of g_{m1} and g_{m2} decreases to $\frac{1}{\sqrt{2}}$ times that of g_{m0}. It causes a rolling shutter effect in output images, which splits the LED light of one circular scan into two consecutive frames, or mixes the LED light of two consecutive circular scans into one frame. To deal with this effect, we obtain a complete image frame illuminated by all of the LEDs from the second frame out of a unit of four frames, in which the LEDs are turned on for the first two frames and then turned off for the next two. The latitude θ_m of the LEDs is changed every four frames.

Experimental results

We evaluated the measurement system in Figure 5 by experiments on the objects shown in Figure 6. All of the objects have a hemispheric shape because they allow us to test the system for a very wide range of surface normal directions. The steel and wood spheres cause mostly specular and diffuse reflection, respectively, whereas the styrofoam sphere causes both. The diameter of the objects is barely wider than the field of view of the correlation camera.

Figures 7–9 show experimental resutls for the hemispheric

Figure 6. *A photograph of the hemispheric objects—styrofoam (left), specular stainless steel (middle) and matte-painted wood (right).*

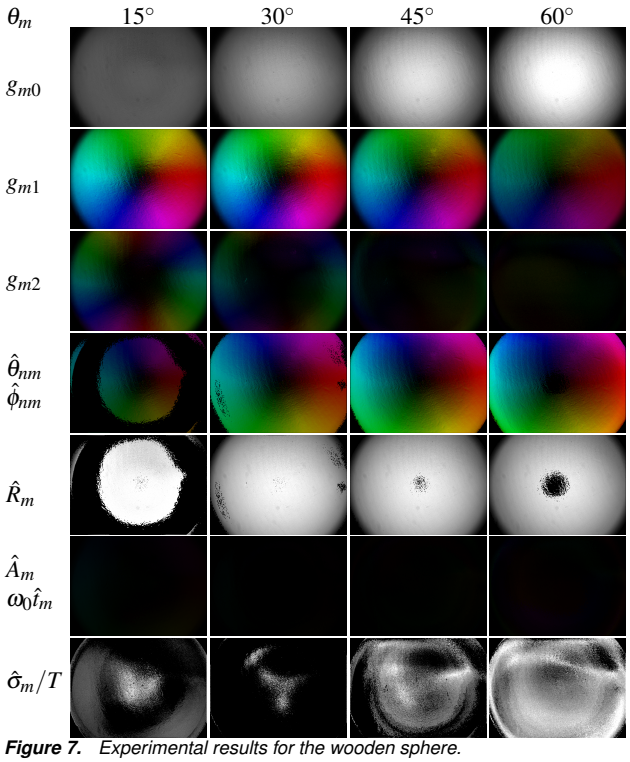

Figure 7. *Experimental results for the wooden sphere.*

objects in Figure 6. In each figure, the three rows from the top show the output images g_{m0}, g_{m1} and g_{m2} from the correlation camera for corresponding latitude θ_m, whereas the four rows below them show the images of estimated parameters of diffuse and specular reflection components. The scanning of LED light started exactly from the left and rotated counter-clockwise during a frame time. The peak time $\hat{t}_m$ is represented in terms of the corresponding phase $\omega_0\hat{t}_m$ in a frame time T, and the peak width $\hat{\sigma}_m$ is normalized by T. The color represents the argument of complex quantities $\angle g_{m1}$ and $\angle g_{m2}$, and the longitude $\hat{\phi}_{nm}$ and $\omega_0\hat{t}_m$, according to the chart in Figure 10. The brightness represents g_{m0}, the magnitude of complex quantities $|g_{m1}|$ and $|g_{m2}|$, the projection of the surface normal vector $\cos\hat{\theta}_{nm}$, and the other scalar parameters A_m and σ_m/T.

Wooden hemisphere

In Figure 7, g_{m2} is nearly zero at $\theta_m = 60°$ all over the image, but begins to deviate from zero in the periphery as θ_m decreases. At high θ_m, the sperical object, which is primarily diffuse, is under the "constant illumination" condition almost everywhere. As θ_m decreases, the object gradually goes into the "partial illumination" condition from the periphery. g_{m0} increases and $|g_{m1}|$ decreases as the latitude of the light source θ_m or the surface normal vector θ_n increases, and $\angle g_{m1}$ changes opposite to the longitude of the

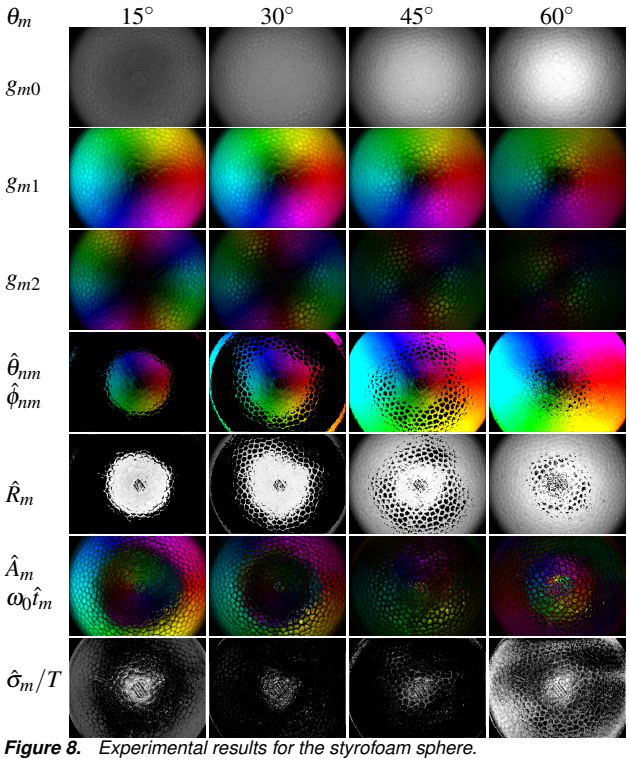

Figure 8. *Experimental results for the styrofoam sphere.*

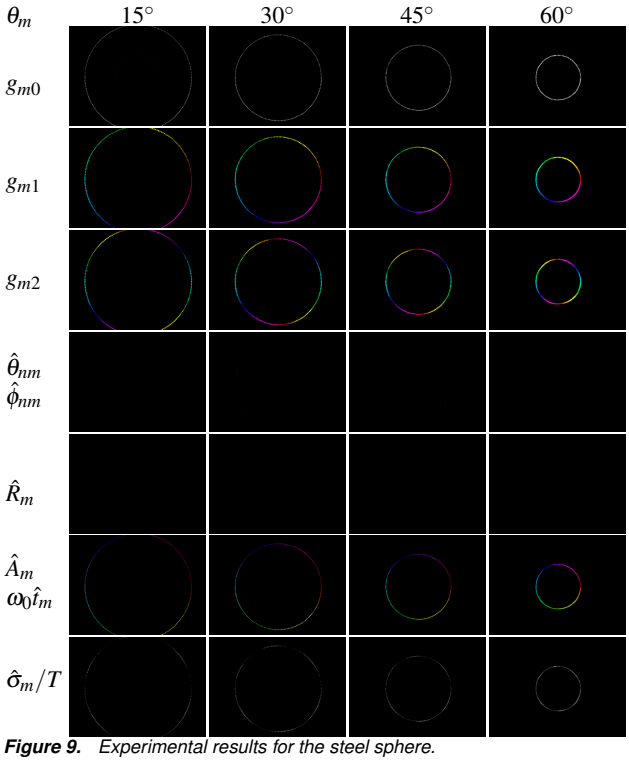

Figure 9. *Experimental results for the steel sphere.*

surface normal vector ϕ_n, as expected from Eq. (15).

The image of the estimated surface normal direction $(\hat{\theta}_{nm}, \hat{\phi}_{nm})$ agrees well with the actual hemispheric shape of the object. The diffuse reflectance $\hat{R}_m$, which is expected to be uni-

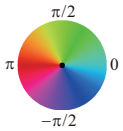

Figure 10. *Color chart for representing the angle.*

form, appears high around the center and slightly decreases toward the periphery. The black areas indicate that R and (θ_n, ϕ_n) were not estimated because the condition $|g_{m2}| < g_{2\min}$ did not hold. The peak height $\hat{A}_m$ of the specular reflection component was estimated to be nearly zero for any θ_m as expected.

Styrofoam hemisphere

The results for the styrofoam sphere in Figure 8 are similar to those for the wooden sphere to some extent, except the effect that appears to have been caused by specular reflection. At $\theta_m = 60^\circ$, g_{m2} does not vanish around the center. The nonzero area is considered to have resulted from specular reflection, because the object is under "constant illumination" in most areas.

Surface normal directions $(\hat{\theta}_{nm}, \hat{\phi}_{nm})$ and diffuse reflectances $\hat{R}_m$ appear reasonably estimated overall. In the periphery, however, the peak height of specular reflection $\hat{A}_m$ seems rather excessively esimated at $\theta_m = 15^\circ$ and 30°, and has the opposite polarity at $\theta_m = 60^\circ$. We consider this phenomenon to have resulted from erroneous separation of diffuse and specular reflection components $\hat{D}_{mk}$ and $\hat{S}_{mk}$. This is further attributed to ununiform LED intensity, which results in excessive estimation of $(\hat{\theta}_{nm}, \hat{\phi}_{nm})$ and $\hat{R}_m$ to introduce errors in $\hat{D}_{mk}$.

Steel hemisphere

The results for the steel sphere in Figure 9 look quite different from those for the wooden and styrofoam spheres. g_{m0}, g_{m1} and g_{m2} all show ring patterns of LED images specularly reflected on the steel sphere, with their diameters shrinking as θ_m increases. The other areas are completely black because the object did not reflect the LED light there. The arguments $\angle g_{m1}$ and $\angle g_{m2}$ monotonically change once and twice, respectively, along the ring patterns opposite to the longitude of the surface normal vector, as expected from Eq. (14).

Surface normal directions $(\hat{\theta}_{nm}, \hat{\phi}_{nm})$ and diffuse reflectances $\hat{R}_m$ were not estimated because the condition where g_{m2} alone is nearly zero did not occur. Although this means that the shape of the object cannot be measured, it can be alternatively obtained because the surface normal vector is known from the image location and the latitude of the LED.

The parameters of specular peak were estimated along the ring patterns of LED images, with the phase $\omega_0 \hat{t}_m$, which is linear to peak time $\hat{t}_m$, changing in accordance with the longitude ϕ_n of the surface normal vector. We, however, have found three problems with the specular component parameters:

1. Peak height $\hat{A}_m$ was ununiformly estimated along the ring patterns.
2. Peak width $\hat{\sigma}_m$ was estimated to be much larger than the actual value, which should be as small as that of a Dirac delta function.
3. The specular commponent parameters were not estimated at six equi-spaced locations along the ring patterns.

We suspect that these problems were caused by ununiform LED intensity and by nonlinear characteristics of the correlation camera in response to pulsed input light.

Conclusion

We proposed a system for simultaneously measuring surface normal vectors and BTF profiles of an object using a correlation camera and a scanning dome light source. We demonstrated by experiments that the implemented system can measure the surface normal vectors and the BTF profile parameters of diffuse and specular reflection components of hemispheric objects with different reflectance characteristics pixel by pixel from a sequence of output images for different latitude of the scanning LED light source.

Acknowledgments

This work was supported by JSPS KAKENHI Grant (Grant-in-Aid for Scientific Research (C)) Number 16K00257.

References

[1] S. R. Marschner *et al.*, *Appl. Opt.*, Vol. 39, No. 16, pp. 2592–2600, 1999.

[2] Y. Mukaigawa *et al.*, *IPSJ Trans. Computer Vision and Applications*, Vol. 1, pp. 21–32, 2009.

[3] M. Ben-Ezra *et al.*, in *IEEE Conf. Computer Vision and Pattern Recognition*, pp. 1–8, Anchorage, AK, 2008.

[4] K. J. Dana *et al.*, *ACM Trans. Graphics*, Vol. 18, No. 1, pp. 1–34, 1999.

[5] Y. Sato *et al.*, *ACM SIGGRAPH '97, Comput. Graphics*, Vol. 31, pp. 379–387, 1997.

[6] H. P. A. Lensch *et al.*, *ACM Trans. Graphics*, Vol. 22, No. 3, pp. 1–27, 2003.

[7] S. Ando and A. Kimachi, *IEEE Trans. Electron Devices*, Vol. 50, No. 10, pp. 2059–2066, 2003.

[8] T. Kurihara *et al.*, *Trans. Soc. Instrument and Control Engineers*, Vol. 48, No. 8, pp. 505–513, 2012 (in Japanese).

[9] T. Kurihara *et al.*, in *Videometrics VIII, Proc. SPIE*, Vol. 5665, pp. 9–16, 2005.

Author Biography

Akira Kimachi received his BS (1993) and PhD (1999) in mathematical engineering and information physics from the University of Tokyo. He worked at the University of Tokyo from 1999 to 2001. Since then he has worked at Osaka Electro-Communication University in Neyagawa, Japan. His work has focused on optical measurement, image sensing and computer vision. He is a member of OSA, SPIE and IEEE.

Motonori Doi received his BS in control engineering from Osaka University (1993) and his PhD in information engineering from Nara Advanced Institute of Science and Technology (NAIST) (1998). He worked at NAIST from 1998 to 2001. Since then he has worked at Osaka Electro-Communication University in Neyagawa, Japan. His work has focused on color/spectral image analysis. He is a member of IS& T and IEEE.

Shogo Nishi received his BS (1998) and PhD (2003) in information engineering from Kagoshima University. He worked at Kagoshima University from 2003 to 2005. Since then he has worked at Osaka Electro-Communication University in Neyagawa, Japan. His work has focused on color/spectral image analysis. He is a member of IS& T.